OPEN ACCESS

GAVIN PUBLISHERS

Biosensors and Bioelectronics Open Access

Research Article

Hu Y, et al. Biosens Bioelectron Open Acc: BBOA-138.

DOI: 10.29011/ 2577-2260.100038

ssDNA@DAPI/Layered Double Hydroxide Biocompatible Composite Ultrathin Film, Its Assembly and Fluorescence Probe for Telomere Detection

Yuehua Hu[1], Ping Zhang[1], Ruili Ma[1], Xiaorang Zhang[1], and Jun Lu[1,2*]

[1]State Key Laboratory of Chemical Resource Engineering, Beijing University of Chemical Technology, Beijing, P. R. China

[2]Beijing Advanced Innovation Center for Soft Matter Science and Engineering, Beijing University of Chemical Technology, Beijing, P. R. China

[*]**Corresponding author:** Jun Lu, State Key Laboratory of Chemical Resource Engineering, Beijing University of Chemical Technology, P. Box 98, Beijing, 100029, P. R. China. Tel: +861064412125; Email: lujun@mail.buct.edu.cn

Citation: Hu Y, Zhang P, Ma R, Zhang X, Lu J (2018) ssDNA@DAPI/Layered Double Hydroxide Biocompatible Composite Ultrathin Film, Its Assembly and Fluorescence Probe for Telomere Detection. Biosens Bioelectron Open Acc: BBOA-138. DOI: 10.29011/ 2577-2260.100038

Received Date: 20 June, 2018; **Accepted Date:** 10 July, 2018; **Published Date:** 16 July, 2018

Abstract

Nucleic Acids, the elemental basis of living organisms, play important roles in the life continuation and development, and also are widely used for pathological diagnosis and analysis, therefore the detection of the nucleic acid sequence is very significant in the biological medicial science. Telomere is a special DNA structure at the end of eukaryotic chromosomal that will shorten with age, which is the most important and accurate indicator of person's aging rate. Therefore, the detection of telomere length is significant for human being. This work describes a systematic study on preparation of Ultrathin Films (UTFs) composite of fluorescent Dye 4',6-Diamidino-2-Phenylindole (DAPI) blending with Single-Stranded DNA (ssDNA) and Layered Double Hydroxides (LDHs) nanosheets by the layer-by-layer method. This new type of bio-inorganic composite material (ssDNA@DAPI/LDHs)n UTFs show uniform and long-range- ordered periodic layered structure that can be used to detect the complementary ssDNA sequence including the telomere squence with various length. The UTFs exhibits excellent selectivity and reversibility, which has potential applications in the field of bioluminescent sensoring materials.

Keywords: Biosensor; DAPI; ssdna; Telomere

Introduction

Nucleic acid is a kind of biological macromolecule mainly distributing in the cell nucleus, which is not only the basic genetic substance, but also has important affect on the protein replication, biosynthesis, and plays a decisive role on a series of major life activities (growth, heredity, variation, etc). DNA is the biological genetic information carrier, with unique sequence for each organism, and plays a key part in the disease diagnosis and identification, thus, the detection of the sequence is crucial in the biological medicine[1,2]. Telomere is a specialized DNA structure at the end of eukaryotic chromosomes used for protecting chromosome ends. Essentially, human telomeres are special DNA structures consisting of repetitive non-transcribed sequences (TTAGGG) and some binding proteins. The length of telomere reflects the cell life and its shortening limits the lifespan of cells. The maintenance of telomere length is a prerequisite for cell division and the average telomere length is usually used to assess telomere function and cancer risk. So it is significant to detect the telomere sequences with different length. At present there are a lot of methods used for telomere DNA detection, and the most commonly ones are Terminal Restriction Fragment (TRF) [3,4], QuantitativePolymerase Chain Reaction (qPCR) [5,6], Quantitative Fluorescence In Situ Hybridization (Q-FISH) [7,8] and Single Telomere Length Analysis (STELA) [9]. Some nanomaterials are also used for DNA detection. Thompson and colleague [10] based the unique properties of Oligonucleotide-Silver Nanoparticle (OSN) conjugates to detecte target DNA by monitoring the colour change of the hybridized conjugates. Maxwell [11] used colloidal gold nanocrystals as both a nano-scaffold and a nano-

quencher, and oligonucleotide molecules labelled with a thiol group at one end and a fluorophore at the other. Binding of target molecules results in a change of fluorescence, then it is possible to recognize specific DNA sequences and single- base mutations in a homogeneous format. Although these methods have their own advantages, almost all of them cannot reuse and require a long response time. For these reasons, a new convenient sensor that can reuse and response quickly is in demand.

4',6-Diamidino-2-Phenylindole (DAPI) as shown in Figure 1 is a fluorescence dye that was usually used for staining live cells and immobilized cells as its penetrability of the cell membrane. It is a common fluorescent marker for DNA with important applications as antiparasitic, antibiotic, antiviral, and anti-cancer drug [12,13]. The existing investigation has shown that the structure of DAPI is similar to some 2-phenyl derivates of classical DNA double helix groove-binding molecules, and binds specifically to AT base pairs [14]. It was widely used as a minor groove fluorescent probe of the DNA double helix [15] giving rise to the so-called "Light-Switch" effect [16,17] as firstly reported by Russell et al [18]. The light-switch behavior refers to the drastic fluorescence emission enhancement upon selectively minor groove binding to dsDNA[19,20]. Actually, DAPI interacted with polynucleotides in a non-univocal manner, both intercalation and minor groove binding modes being possible [21-23], and to specifically change its photophysical properties according to the different environment.It can be combined strongly with DNA in the cell nucleus and lead to a fluorescence enhanced contrast.

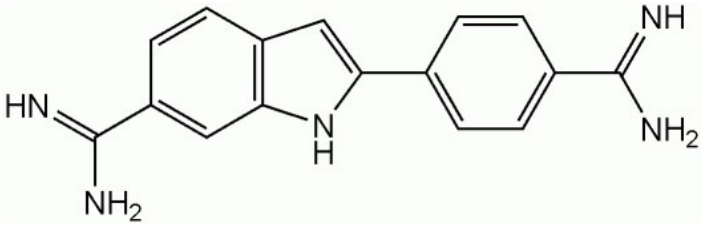

Figure1: The structure of DAPI.

Layered Double Hydroxides (LDHs) are large class of layered inorganic solid solution materials, which can be described by the general formula $[M^{II}_{1-x}M^{III}_{x}(OH)_2]^{z+}A^{n-}_{z/n}\cdot yH_2O$ (M^{II} and M^{III} are divalent and trivalent metals respectively; A^{n-} is the anion) [24,25]. The synthesis and intercalation assembly of LDH, especially the preparation and the development of the assembled films based on LDHs, attracted widespread interest and attention in the field of functional materials research [26]. As a typical anionic inorganic layered material, LDHs crystallites can be exfoliated into nanosheets due to their facile swelling characteristics in the organic solvent [27-29], which provides the building blocks for the construction of multifunctional composite Ultrathin Film (UTF) material. The LDHs exfoliated nanosheets are transparent, biocompatible and UV-light proof [30,31], therefore, it can be used as a molecular container to stabilize and immobilize the biological macromolecules within the interlayer spaces. Currently, the DNA intercalated LDH displayed novel functions and has drawn more and more attention. Shi [32] reported a layer-by-layer self-assembly method to fabricate a highly oriented DNA intercalated LDH film, and its application in chiroptical switch was studied and demonstrated via intercalation/ deintercalation of an achiral molecule into the DNA cavity. Léa Desigaux [33], synthesized LDH/DNA hybrids by coprecipitation method, which is a new way to synthesize new labile, nonviral gene delivery systems. Chen [34] used a constant vibriation method to fabricate the DNA-LDH nanohybrids composed by electrostatic forces, the DNA-LDH nanohybrids exhibited DNA-enhanced peroxidase-like activity and could be applicated in H_2O_2 and glucose sensing. Baccar [35] reported the development of an impedimetric DNA-biosensor based on LDH for the detection of long ssDNA sequences, which showed a high sensitivity for the detection of 80 bases long DNA complementary sequences.

In this paper, we demonstrated the successful fabrication of new type of biocompatible layered composite material $(ssDNA@DAPI/LDH)_n$ UTFs by the co-assembly method as we reported previously [36-38]. The UTFs show uniform and long-range-ordered periodic layered structure. This composite system can detect the complementary ssDNA sequence by DAPI fluorence enhancement, and have good selectivity for the long complementary ssDNA sequence like telomere compared to a range of other ssDNA sequence. In addition, the $(ssDNA@DAPI/LDH)_n$ UTFs displayed a well stability and reversiblity fluorescence response for the complementary ssDNA sequence, which indicates that this film can be a novel potential fluorescence sensor for the specific ssDNA sequence.

Experiment

Materials

All the DNA primers were purchased from Taihe Biotechnology Co., Ltd, and the primers ID and sequences were shown in Table 1. the 4',6-Diamidino-2- Phenylindole (DAPI) was purchased from J&K Chemical. Co. Ltd. Analytical grade $Mg(NO_3)_2\cdot 6H_2O$, $Al(NO_3)_3\cdot 9H_2O$, HCl, HNO_3, $NH_3\cdot H_2O$, ethanol, 95~98 wt% H_2SO_4, 30 wt% H_2O_2, NaCl and NaOH were purchased from Beijing Chemical Co. Ltd. Tris (hydroxymethyl) aminomethane was purchased from Shang-hai Aladdin Bio- Chem Technology Co., Ltd. Polydimethyldiallyl-Ammonium Chloride (PDDA, Mw = 100, 000-200, 000)

and Poly (Styrene sulfonic acid) (PSS, Mw=70, 000) were purchased from J&K Chemical. Co. Ltd. All of these reagents were used without further purification. Deionized and decarbonated water was used throughout the experimental process. Ultrapure water was made by the Millipore ultrapure water purifier from RephiLe Bioscience Co., Ltd.

	Primer ID	5' Sequences 3'	Bases number
Conventional base complementary sequence	$A_{59,\ 43,\ 27}$	5'- $(AAAG)_{14,10,6}$ AAA-3'	59, 43, 27
	$A_{10,\ 6}$	5'- $(AAAG)_{2,1}$ AA-3'	10, 6
	$A_{12,\ 8,\ 4}$	5'- $(AAAG)_{3,2,1}$ -3'	12, 8, 4
	$T_{59,\ 43,\ 27}$	5'- TTT $(CTTT)_{14,10,6}$ -3'	59, 43, 27
	$T_{10,\ 6}$	5'- TT $(CTTT)_{2,1}$ -3'	10, 6
	$T_{12,\ 8,\ 4}$	5'- $(CTTT)_{3,2,1}$ -3'	12, 8, 4
The telomere sequence	$tC_{54,\ 36,\ 18,\ 12}$	5'-$(CCCTAA)_{9,6,3,2}$ -3'	54,36,18,12
	tC_{10}	5'-CCCTAACCCT-3'	10
	tC_{8}	5'-CCCTAACC-3'	8
	tC_{6}	5'-CCCTAA-3'	6
	$tG_{54,\ 36,\ 18,\ 12}$	5'-$(TTAGGG)_{9,6,3,2}$ -3'	54,36,18,12
	tG_{10}	5'-TTAGGGTTAG-3'	10
	tG_{8}	5'-TTAGGGTT-3'	8
	tG_{6}	5'-TTAGGG-3'	6

Table 1: Sequences and bases number of the primers used in this work.

Fabrication of the $(ssDNA@DAPI/LDH)_n$ UTFs

A colloidal LDH suspension was prepared according to the Separated Nucleation And Aging Steps (SNAS) method reported previously [39,40], 80 mL NaOH (0.18 mol) solution and 70 mL salt solution (0.06 mol $Mg(NO_3)_2 \cdot 6H_2O$ and 0.03 mol $Al(NO_3)_3 \cdot 9H_2O$) were simultaneously added to a colloid mill and mixed for 2 min with a rotor speed of 4000 rpm. The resulting slurry was removed and heated in 100 mL PTFE-lined autoclave at 110°C for 24 hours. The product was washed three times with deionized and decarbonated water, then a stable homogeneous MgAl-LDH suspension with a narrow size distribution can be obtained after washing for 4 times. The concentration of LDH colloidal particles used for the thin film fabrication was 0.10 wt %.

The quartz substrates were cleaned in a mixed solution with concentrated H_2SO_4/30% H_2O_2 (vol : vol = 7 : 3) for 30 min and then washed by anhydrous alcohol and deionized water thoroughly. To improve the adhesion between the film and the substrate, the cleaned substrates were dipped into a cationic PDDA solution (10 g/L) for 30 min and thoroughly rinsed with distilled water and dried in a nitrogen gas flow. Then the substrates were dipped into an anionic PSS solution (10 $g \cdot L^{-1}$) for 30 min and thoroughly rinsed with distilled water and dried in a nitrogen gas flow. This treatment made the quartz substrates pre-assembled with one layer polymer UTF. The preparation of the $(ssDNA@DAPI/LDH)_n$ multilayer UTFs were carried out as the follows: the pretreated quartz substrate was immersed in the LDH colloidal suspension (1 $g \cdot L^{-1}$) for 15 min followed by through washing with deionized water and drying in a nitrogen gas flow at room temperature, and then the substrate was treated with ssDNA@DAPI solution (ssDNA: DAPI = 0.04 $mg \cdot mL^{-1}$: 0.02 $mg \cdot mL^{-1}$, Tris buffer solution pH = 8) for 15 min, washed several times with deionized water and dried in a nitrogen gas flow for 2 min at room temperature. The $(ssDNA@DAPI/LDH)_n$ UTFs were fabricated by alternatively deposition of LDH colloidal suspension and ssDNA@DAPI solution for n cycles, and after every deposition, the UTFs were washed several times with deionized water and dried under a nitrogen gas flow for 2 min at room temperature.

The quartz substrates with $(ssDNA@DAPI/LDH)_n$ UTFs were put into the quartz cuvette. The fluorescence emission spectra were measured after adding a certain amount of buffer solution or testing ssDNA each time. The test process for the reversibility is as following: $(ssDNA@DAPI/LDH)_n$ was put into the quartz cuvette, the fluorescence emission spectra were measured after adding a certain amount of buffer solution and a certain amount of the tested ssDNA. Then, suck out of the solution, replenish the same amount of buffer solution, and put quartz cuvette in a thermostat water bath for heating 5 min at 75°C. Thirdly, suck out of the solution in the cuvette and record the fluorescence emission spectra after adding the same amount

of buffer solution and the tested ssDNA. Repeat the above operations several times to study the stability of the UTFs. The fluorescence emission spectra of UTFs were measured after adding a certain amount of different ssDNA sequences for testing the selectivity of the UTFs.

Characterization

The UV-vis absorption spectra were collected on a Shimadzu U-3600 spectrophotometer with the slit width of 1.0 nm. The fluorescence spectra were obtained on a FL-4600 fluorospectrophotometer with an identical condition for comparison. The Circular Dichroism (CD) spectra were recorded using a JASCO J-815 circular dichroism spectrometer with a slit width of 1.0 nm from 185 to 500 nm. The polarized fluorescence spectra were recorded with an Edinburgh Instruments' FL 900 fluorimeter. The small-angle XRD patterns of the films were obtained with a Rigaku 2500VB2+ PC diffractometer using Cu Kα radiation (λ= 1.541844 Å, 2θ = 0.5 − 8°) at 40 kV, 50 mA, with the step-scanned mode with 0.04°(2θ) per step and count time of 10 s per step. A Scanning Electron Microscope (SEM Zeiss Supra 55) was used to investigate the morphology of LDH and the thin films.

Result and Discussion

The Assembly of (ssdna@DAPI/LDH)$_n$ UTFs

ssDNA is a kind of biological polyanion, which is conducive to assemble with positive-charged LDH nanosheets by electrostatic interaction. DAPI is a small fluorescent molecule. It mixes with the ssDNA polyanions can be assembled with LDH nanosheets via the co-assembly method as reported by our previous work (Scheme 1) [36-38].

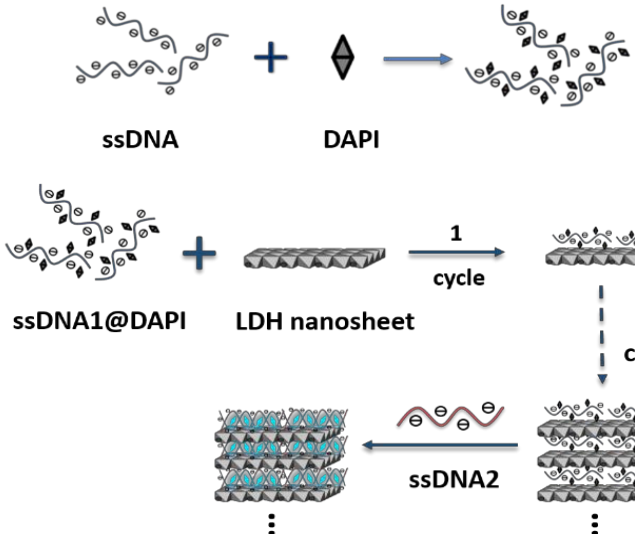

Scheme 1: The assembly scheme of the (ssDNA@DAPI/LDH)$_n$ UTFs.

The assembly process of the (ssDNA@DAPI/LDH)$_n$ UTFs deposited on quartz substrates was similar to the ordinary electrostatic assembly of polyanions with LDHs nanosheets, except that the LDH nanosheets were prepared by SNAS method as reported previously [39,40] and the XRD pattern and SEM image of the Mg_2Al-NO_3 LDH powders were shown in Figure S1. The multilayer assembly process of the (ssDNA-A59@DAPI/LDH)$_n$ (n = 4 − 16), (ssDNA- T59@DAPI/LDH)$_n$ (n = 4 − 16), (ssDNA-tC54@DAPI/LDH)$_n$ (n = 3 − 12) UTFs and (ssDNA- tG54@DAPI/LDH)$_n$ (*n* = 3 − 12) on quartz substrates were were monitored by UV-vis absorption spectra (Figure 2) and fluorescence spectra (Figure 3). The absorption intensities of the bands at 258, 267 and 348 nm for (ssDNA- A59@DAPI/LDH)$_n$ and (ssDNA-T59@DAPI/LDH)$_n$ (n = 4 − 16) correlated nearly linearly with the number of bilayers n (Figures 2A, B), indicating the UTFs were LbL linearly grown. The absorption bands at 258 and 267 nm of the UTFs are mainly attributed to the characteristic absorption of ssDNA, and the absorption band at 348 nm of the UTFs may be attributed to that of DAPI, all of which corresponded to the those of pristine ssDNA and DAPI solution (Figures S2 and S3A).

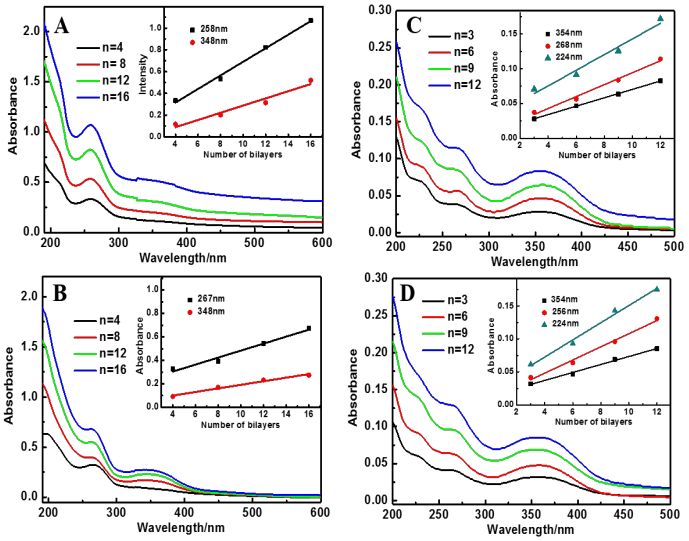

Figures 2(A-D): Absorption spectra of **(A)** (ssDNA-A59@DAPI/LDH)$_n$ and **(B)** (ssDNA- T59@DAPI/LDH)$_n$ (n = 4-16) UTFs, insert: the plot of the absorbance vs. n at 258 and 348 nm of the UTFs. **(C)** (ssDNA- tC54@DAPI/LDH)$_n$ and **(D)** (ssDNA-tG54@DAPI/LDH)$_n$ (n = 3- 12, λex= 370 nm) UTFs, insert: the plot of the fluorescence intensity vs. n at 224,264 and 354 nm of the UTFs.

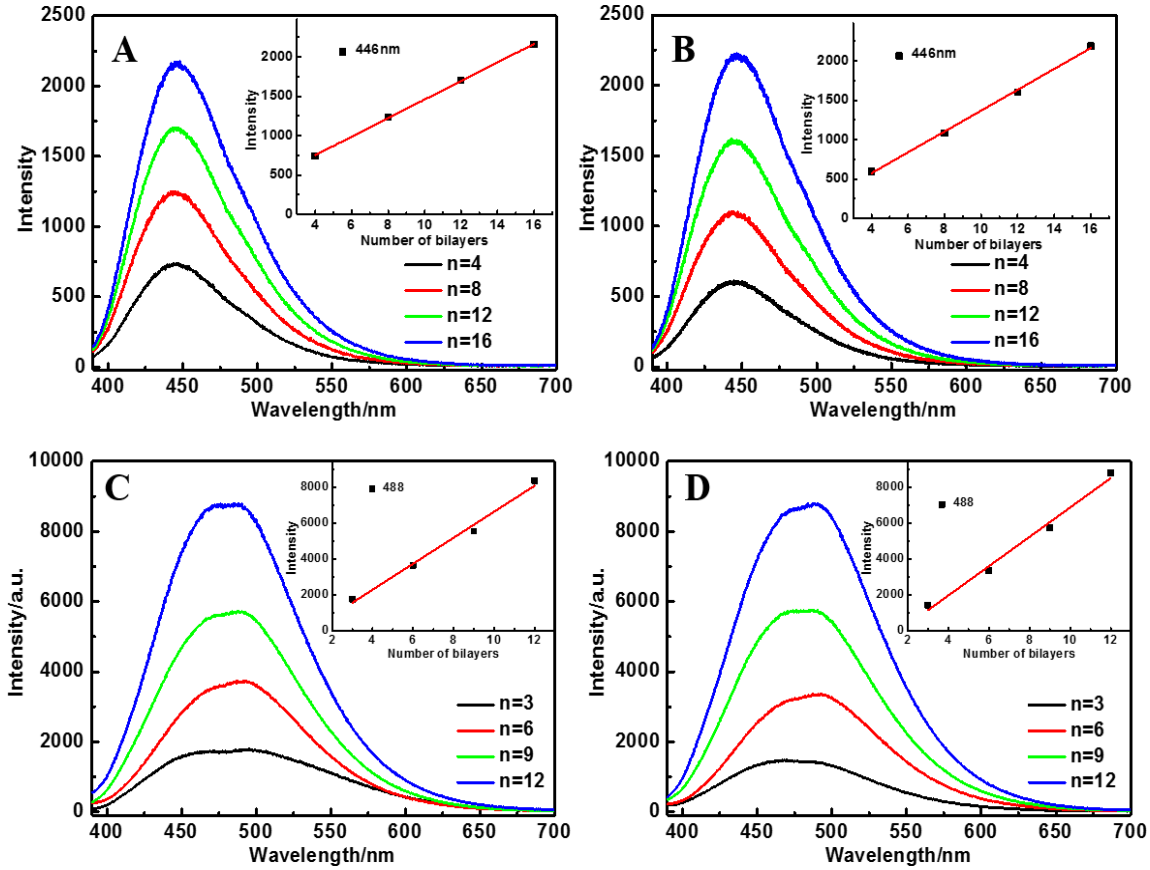

Figures 3(A-D): Fluorescence spectra of **(A)** (ssDNA-A59@DAPI/LDH)$_n$ and **(B)** (ssDNA- T59@DAPI/LDH)$_n$ (n = 4-16) UTFs, **(C)** (ssDNA- tC54@DAPI/LDH)$_n$ and **(D)** (ssDNA-tG54@DAPI/LDH)$_n$ (n = 3-12) UTFs, insert: the plot of the fluorescence intensity of the UTFs vs. the bilayers number at the maximum emission wavelength.

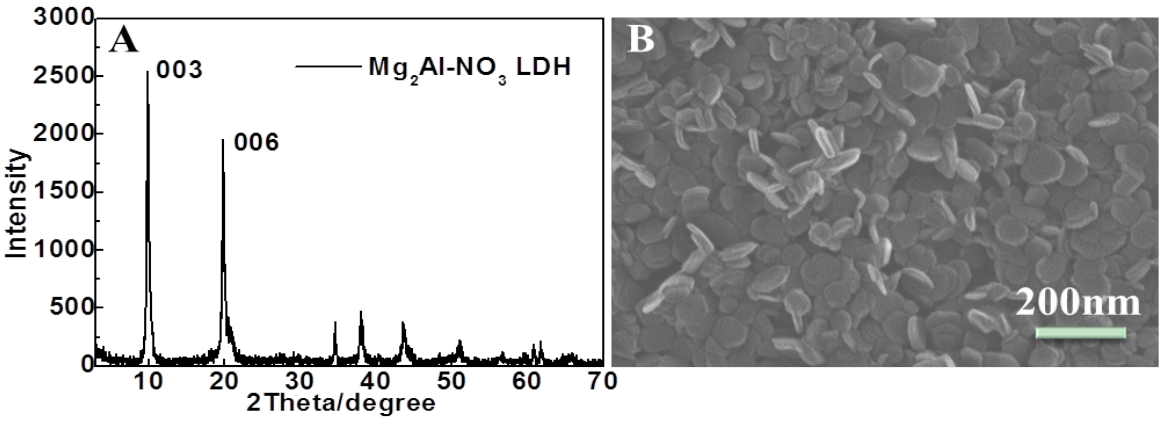

Figure S1: (A) XRD pattern and **(B)** SEM image of $Mg_2Al\text{-}NO_3$ LDH powders prepared by SNAS method.

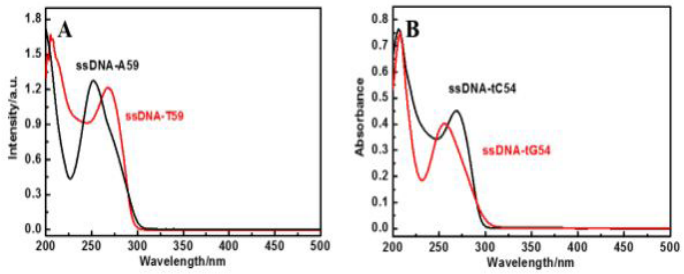

Figures S2(A,B): UV-vis absorption spectra of **(A)** ssDNA-A59 and ssDNA-T59 **(B)** ssDNA-tC54 and ssDNA- tG54.

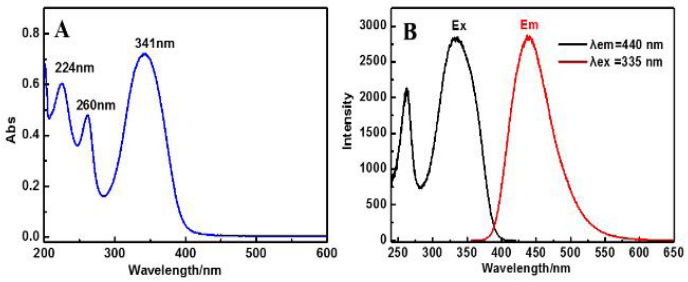

Figures S3(A,B): (A) UV-vis absorption spectra and **(B)** fluorescence spectra of DAPI.

The intensity of the sharp luminescence peak with a maximum at 446 and 488 nm of the $(ssDNA\text{-}A59@DAPI/LDH)_n$ (n = 4 − 16), $(ssDNA\text{-}T59@DAPI/LDH)_n$ (n = 4 − 16) (Figure 3A,B), $(ssDNA\text{-}tC54@DAPI/LDH)_n$ (n = 3 − 12) and $(ssDNA\text{- }tG54@DAPI/LDH)_n$ (n = 3 − 12) (Figure 3C,D) UTFs also displays a monotonic increase with n, which further suggests that a stepwise and regular deposition procedure with almost equal amounts of ssDNA@DAPI and LDH incorporated in each cycle. And the fluorescence emission wavelength of the $(ssDNA@DAPI/LDH)_n$ UTFs was similar to that of the original DAPI solution (Figure S3B), suggesting the absence of aggregates of DAPI in the $(ssDNA@DAPI/LDH)_n$ UTFs throughout the whole assembly. The absorption and nd fluorescence spectra indicated the successful co-assembly of ssDNA@DAPI with LDH nanosheets on the quartz substrate and the regular growth during the assembly process. The small angle XRD patterns show a sharp Bragg peaks at 2θ=1.20˚, 1.24˚, 1.23˚ and 1.28˚ for $(ssDNA\text{ -A59@DAPI/LDH})_{40}$, $(ssDNA\text{- T59@DAPI/LDH})_{40}$, $(ssDNA\text{-tC54@DAPI/LDH})_{40}$ UTFs and $(ssDNA\text{-tG54@DAPI/LDH})_{40}$ UTFs respectively (Figure 4), indicating an ordered periodical structure perpendicular to the substrate with a period length of 7.12 nm, 7.35 nm, 7.17 nm, 6.89 nm, respectively.

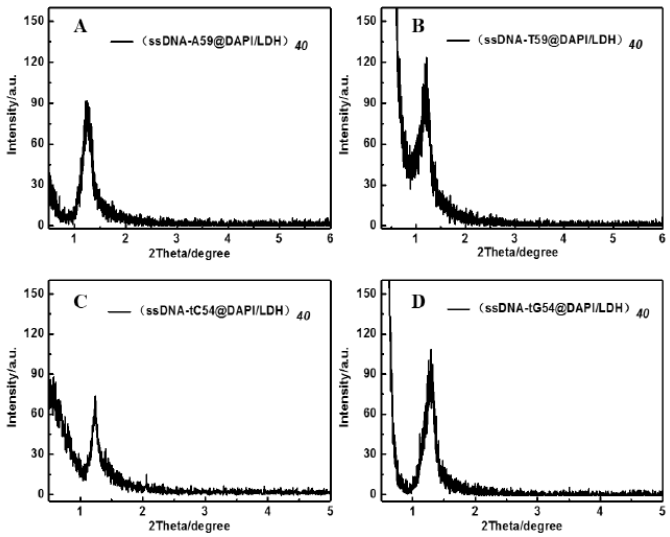

Figure 4: The small-angle XRD patterns of **(A)** $(ssDNA\text{-}A59@DAPI/LDHs)_{40}$, **(B)** $(ssDNA\text{-}T59@DAPI/LDHs)_{40}$, **(C)** $(ssDNA\text{- }tC54@DAPI/LDH)_{40}$ and **(D)** $(ssDNA\text{- }tG54@DAPI/LDH)_{40}$ UTF.

Morphology and Structure Characterization of the $(ssDNA@DAPI/\ LDH)_n$

The CD spectra were measured to characterize the secondary structure of the embedded ssDNA in the $(ssDNA\text{-}@DAPI/LDH)_8$ UTFs (Figure 5). The strong negative band at 258 nm and positive band at 221 nm of the $(ssDNA\text{- }A59@DAPI/LDH)_n$ UTF (Figure 5A), corresponding to the negative band at 250 nm and positive band at 217 nm of the original ssDNA-A59 solution , indicated the secondary structure of the ssDNA-A59 in the UTFs had changed obviously, which was mainly attributed to the electrostatic interaction between the ssDNA- A59 and LDH nanosheets. It is also the case for the secondary structure of ssDNA- tC54 in the UTFs which has also changed due to the electrostatic interaction between the ssDNA-tC54 and LDH nanosheets (Figure 5C). Nevertheless, the CD spectra of $(ssDNA\text{-}T59@DAPI/LDH)_n$ and $(ssDNA\text{-}tG54@DAPI/LDH)_n$ show great changes compared with the of the original ssDNA-T59 and ssDNA-tG54 solution respectively (Figure 5C,D). The positive band nearly disappeared and negative band became stronger. This phenomenon may be not only due to the interaction between the ssDNA and LDH nanosheets but also related to the special interaction betweenthe specific ssDNA sequence, the interlayer DAPI and the host lamellar LDH nanosheets.

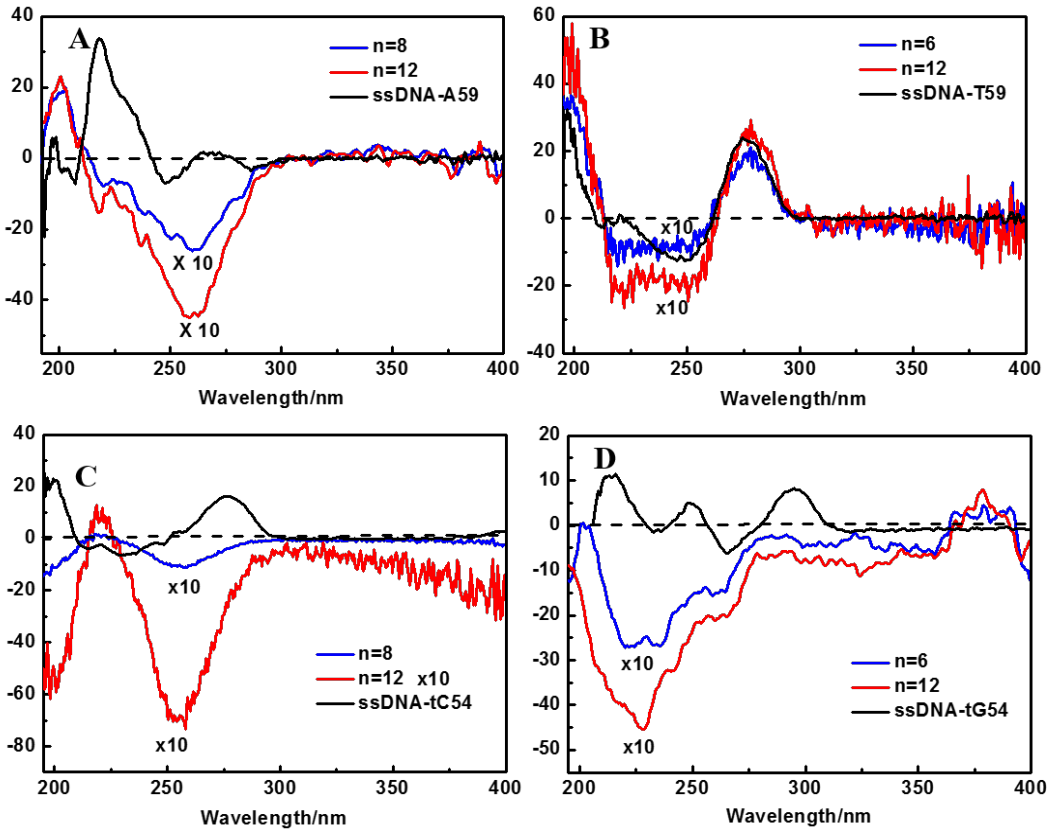

Figures 5(A-D): CD spectra of **(A)** ssDNA-A59, $(ssDNA\text{-}A59@DAPI/LDH)_n$ (n = 8, 12) UTFs, **(B)** ssDNA-T59, $(ssDNA\text{-}T59@DAPI/LDH)_n$ (n = 8, 12) UTFs, **(C)** ssDNA- tC54, $(ssDNA\text{- }tC54@DAPI/LDH)_n$ (n = 6, 12) UTFs and **(D)** ssDNA- tG54, $(ssDNA\text{- }tG54@DAPI/LDH)_n$ (n= 6, 12) UTFs. All the peak intensity of UTFs are magnified by 10 times.

The SEM images were measured to probe the surface morphology and the thickness of the $(ssDNA@DAPI/LDH)_n$ UTFs. The top-view of SEM image shows that the film surface is microscopically continuous and homogenous and the surface roughness of the UTFs increase with the bilayer number n (Figure 6). The side view of SEM images (Figure 6) show that the thickness of the $(ssDNA@DAPI/LDH)_n$ UTFs approximately linearly increased upon the bilayer number n, and the average thickness of one bilayer of $(ssDNA\text{- }A59@DAPI/LDH)_n$$(ssDNAT59@DAPI/LDH)_n$,(ssDNA-

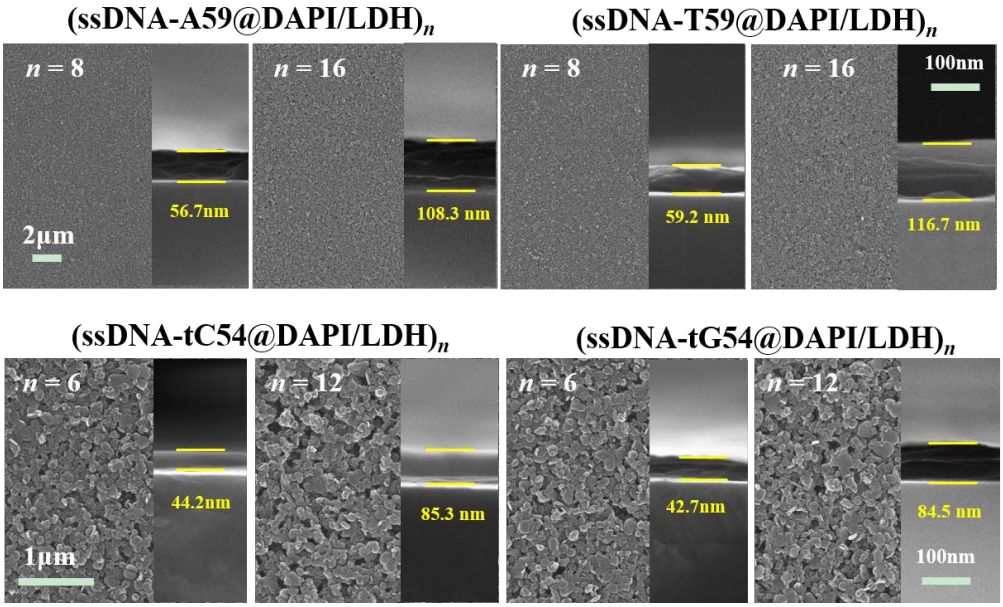

Figure 6: Top and side-view SEM images of $(ssDNA\text{-}A59@DAPI/LDH)_n$ (n = 8-16), $(ssDNA\text{- }T59@DAPI/LDH)_n$ (n = 8-16), $(ssDNA\text{-}tC54@DAPI/LDH)_n$ (n = 6-12) and $(ssDNA\text{- }tG54@DAPI/LDH)_n$ (n = 6-12) UTFs.

$tC54@DAPI/LDH)_n$ UTFs and $(ssDNA\text{-}tG54@DAPI/LDH)_n$ UTF can be estimated to be 6.9, 7.3, 7.19 and 7.07 nm, respectively, which are approximately close to the basal spacing observed by small-angle XRD (ca. 7.12 - 7.35 nm) (Figure 4). Moreover, the surface morphology keeps homogenous and continuous and the bilayer number *n* can be up to 40 at least. This further confirms that the $(ssDNA@DAPI/LDH)_n$ UTFs present uniform and periodic layered structure, in agreement with the behaviors revealed by their absorption and fluorescence spectra.

Selective Fluorescence Response for the Conventional Complementary ssDNA Sequence

The fluorescence intensity of DAPI molecules bound to Double- Stranded DNA (dsDNA) can be enhanced by about 20-fold, compared with its free state [41]. Therefore, the presence and the amount of dsDNA can be detected depending on the fluorescence intensity. Based on this property of DAPI, we studied the fluorescence response of the $(ssDNA@DAPI/LDH)_n$ UTFs for different lengths of its complementary ssDNA sequences. Experimentally, the $(ssDNA\text{- }A59@DAPI/LDH)_n$ and $(ssDNA\text{-}T59@DAPI/LDH)_n$ UTFs both exhibited a significantly fluorescence variation for its complementary one's with different lengths (Figure 7). It is obvious that the UTFs exhibit a significantly fluorescence enhancement for these complementary ssDNA sequences with more than 10 bases, however, there is no obvious change for the shorter complementary ssDNA sequences less than 10 bases. This implied that the DNA double helix structure can form within the interlayers of the LDHs UTFs for the ssDNA with more than 10 base pairs, and DAPI can interact with them as a groove binding mode, to result in the enhanced fluorescence of DAPI. This indicated that the $(ssDNA@DAPI/LDH)_n$ UTFs can be used to detected different length of complementary ssDNA sequence with 10 or above bases.

To study the selectivity of fluorescence response for the complementary ssDNA sequence, we further research the fluorescence response of the $(ssDNA@DAPI/LDH)_n$ UTFs for different ssDNA sequence. Figure 7C illustrates the fluorescence intensity change of $(ssDNA\text{-}A59@DAPI/LDH)_n$ and $(ssDNA\text{-}T59@DAPI/LDH)_n$ UTFs toward various ssDNA sequence.

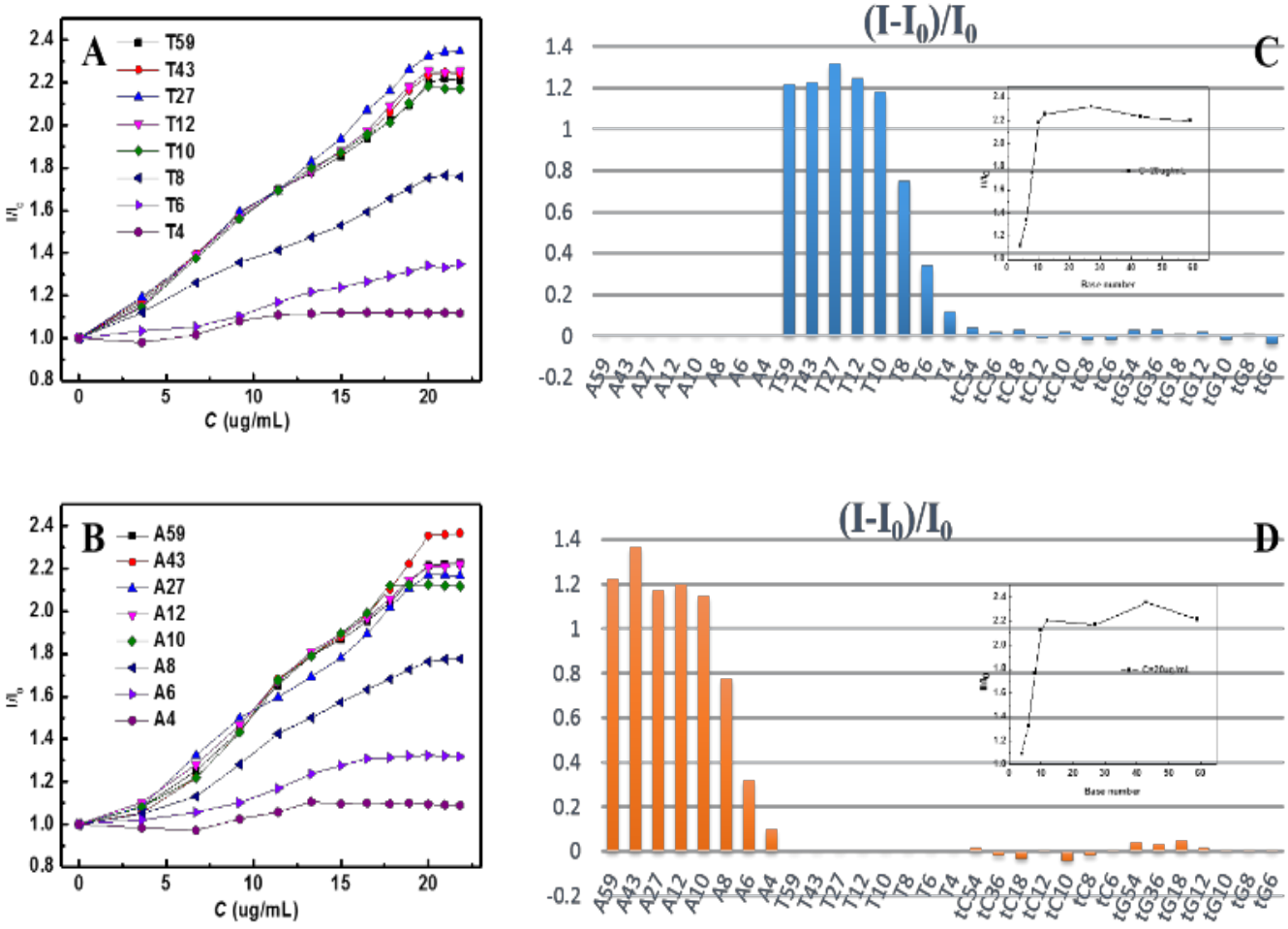

Figures 7(A-D): Plots of the maximal fluorescence intensity of **(A)** (ssDNA-A59@DAPI/LDH)$_8$, **(B)** (ssDNA-T59@DAPI/LDH)$_8$ versus the different concentration of their corresponding complementary ssDNA sequence, and the fluorescence intensity changes $(I-I_0)/I_0$ of **(C)** (ssDNA-A59@DAPI/LDH)$_8$ and **(D)** (ssDNA-T59@DAPI/LDH)$_8$ for different ssDNA sequences(20 μg/mL). Insert: the plot of the fluorescence intensity of the UTFs vs. the base number of their corresponding complementary ssDNA sequence at 20ug/mL.

Remarkably, there is no obvious fluorescence intensity change for the different ssDNA sequence except the long complementary ssDNA sequences. The result indicated that the (ssDNA@DAPI/LDH)$_n$ UTFs can be used as a biosensor for selective detection of the long complementary ssDNA sequences over a range of other ssDNA sequences.

Selective Fluorescence Response for the Telomere Sequence

In order to further study the fluorescence response for thetelomere sequence with different length, we designed the fragments the same as the telomere sequence and also assembled with DAPI into the UTFs. Experimentally, the (ssDNA- tC54@DAPI/LDH)$_n$ and (ssDNA- tG54@DAPI/LDH)$_n$ UTFs both exhibit a significantly fluorescence variation for different lengths of complementary telomere ssDNA sequence (Figure 8). The fluorescence of the UTFs enhanced significantly by the complementary telomere DNA sequence with more than 10 bases, otherwise, there is no obvious fluorescence variation for the telomere sequence less than 10 bases.

In addition, the selectivity of fluorescence response for the complementary telomere sequence is similar to the conventional base complementary ssDNA sequence that was described hereinbefore. As it is shown in Figure 8, the fluorescences of (ssDNA-tC54@DAPI/LDH)$_n$ and (ssDNA- tG54@DAPI/LDH)$_n$ UTFs both exhibit enhancement to some extent toward the telomere sequence with different lengths. Therefore, the UTFs is expected to be a new biosensor for the selective detection of long complementary telomere sequence.

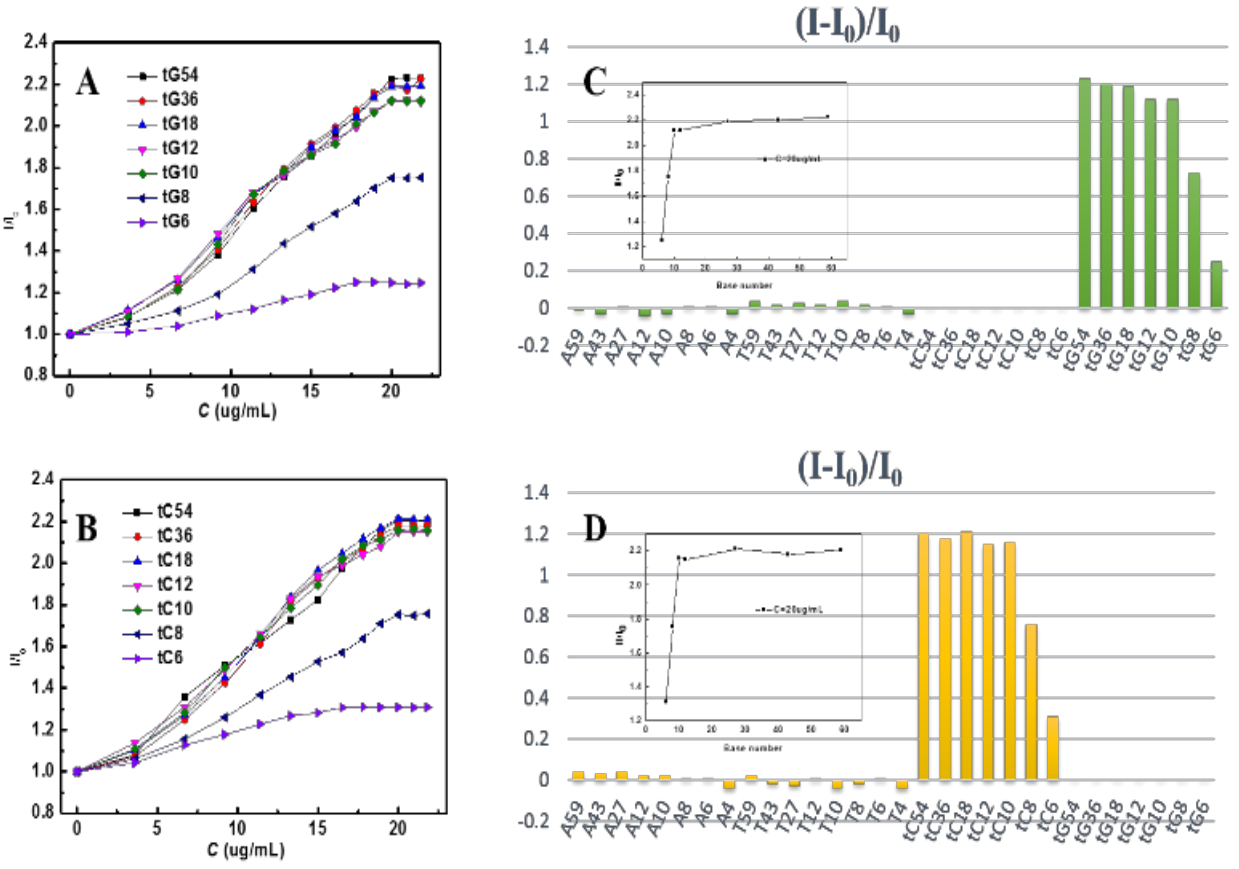

Figure 8: Plots of the maximal fluorescence intensity of **(A)** (ssDNA-tC59@DAPI/LDH)$_8$, **(B)** (ssDNA-tG59@DAPI/LDH)$_8$ versus the different concentration of their corresponding complementary ssDNA sequence, and the Fluorescence intensity changes $(I-I_0)/I_0$ of **(C)** (ssDNA- tC 59@DAPI/LDH)$_8$, **(D)** (ssDNA- tG 59@DAPI/LDH)$_8$ for different ssDNA sequences(20 μg/mL). Insert: the plot of the fluorescence intensity of the UTFs vs. the base number of their corresponding complementary ssDNA sequence at 20μg/mL.

Reversible Fluorescence Response for the Complementary ssDNA Sequence

To study the reversibility of fluorescence response for the complementary ssDNA sequence, we further investigate the fluorescence changes of the $(ssDNA@DAPI/LDH)_n$ UTFs with or without the complementary ssDNA sequence by heating the composite system to break the double helix structure. Taking $(ssDNA\text{-}A59@DAPI/LDH)_8$ and $(ssDNA\text{-}tC54@DAPI/LDH)_8$ UTF as examples, the UTFs showed reversible fluorescence responses with or without the complementary ssDNA sequence (Figure 9A). In order to investigate the interference of temperature for the reversibility experiment, the fluorescence spectra (Figure S4) of DAPI and ssDNA@DAPI solution were recorded at different temperature (room temperature and 75℃ , respectively), and showed no change with the variation of temperature, this result further indicated that the fluorescence enhancement is only due to the adding of the complementary ssDNA sequence. Moreover, after four cycles of alternatively treatment by heating or adding complementary ssDNA sequence, the UTFs still keep well fluorescence properties (Figure 9B), confirming the stability and reversiblity of the $(ssDNA@DAPI/LDH)_n$ UTFs for the complementary ssDNA sequence detection, which indicates that this film can be a novel potential fluorescence reusable sensor for the specific ssDNA sequence.

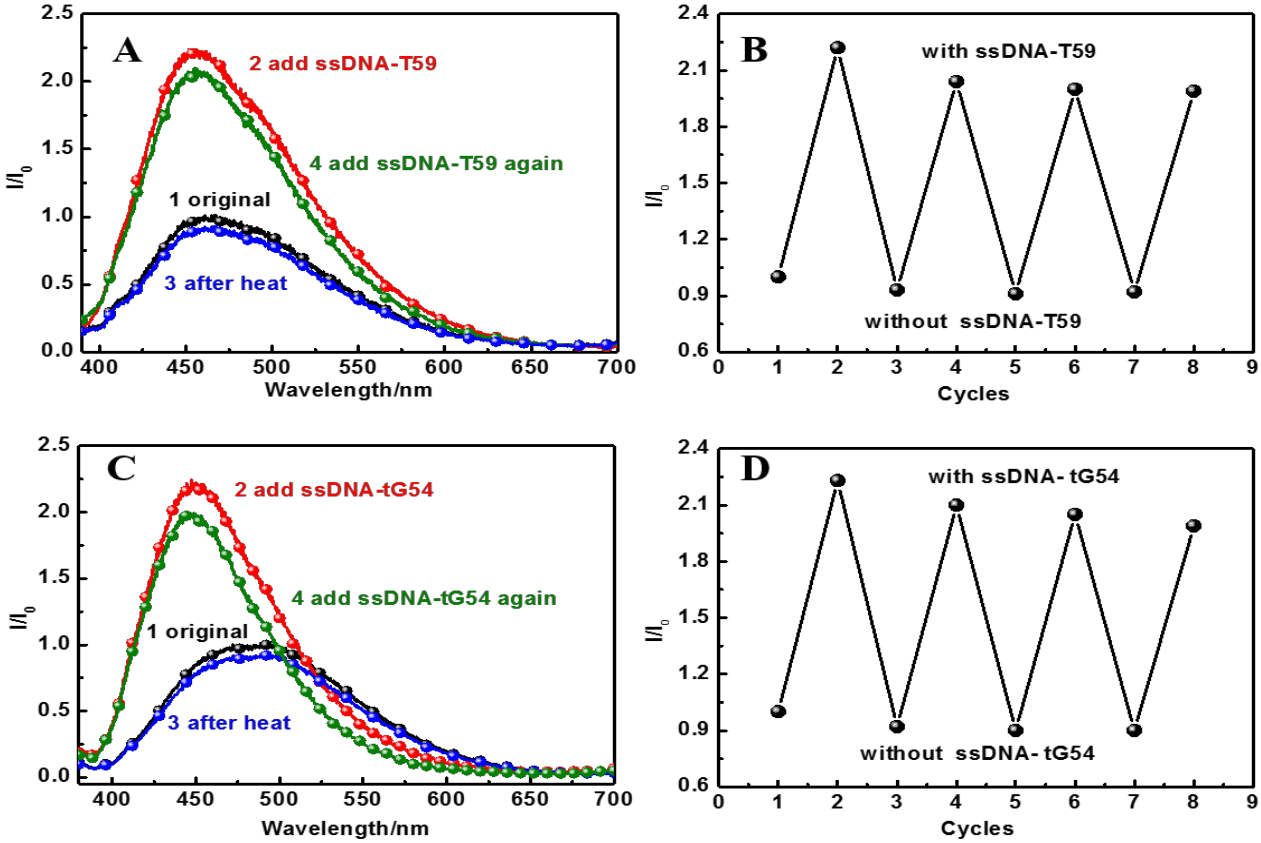

Figures 9(A-D): Fluorescence spectra of **(A)** $(ssDNA\text{-}A59@DAPI/LDH)_8$ and **(C)** $(ssDNA\text{-}tC54@DAPI/LDH)_8$ UTF with different conditions, fluorescence intensity of **(B)** $(ssDNA\text{-}A59@DAPI/LDH)_8$ and **(D)** $(ssDNA\text{-}tC54@DAPI/LDH)_8$ UTF subjected to the alternative treatment by heating or adding complementary ssDNA, respectively.

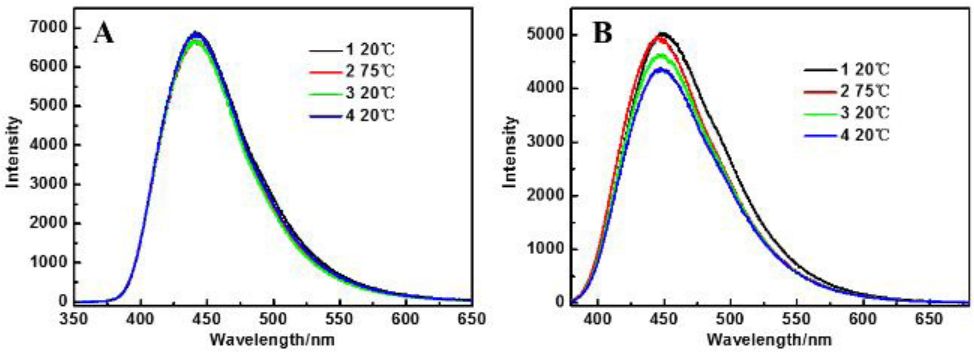

Figure S4: Fluorescence spectra of **(A)** DAPI and **(B)** DAPI@ssDNA-A59 solution at different temperature.

Conclusion

In summary, the small molecule dye DAPI blending with ssDNA was successfully co-assembled with LDH nanosheets to form $(ssDNA@DAPI/LDH)_n$ biocompatible UTFs by the LbL assembly technique, which realized the immobilization of ssDNA and DAPI. It was found that the obtained $(ssDNA@DAPI/LDH)_n$ UTFs show uniform and long-range-ordered periodic layered structure. This UTFs can sensor fluorescence enhancement of the complementary ssDNA sequence and have remarkable selectivity for the long complementary ssDNA sequence, and telomere sequence over a range of other ssDNA sequence. It was speculated that the detection mechanism is attributed to the formation of double helix structure by base pairing of complementary ssDNA sequence and the groove binding mode between DAPI and the double helix structure within the interlayers of the UTFs. In addition, the $(ssDNA@DAPI/LDH)_n$ UTFs displayed a well stability and reversiblity fluorescence response for the complementary ssDNA sequence, which indicates that this film can be a novel potential fluorescence sensor for the specific ssDNA sequence. However, it still limits the application due to the long preparation period of the UTFs. In the future, we will further optimize preparation process of the UTFs, in order to its better application for telomere offline testing.

Acknowledgements

This study was supported by the 973 Program (grant no.2014CB932101), the National Natural Science Foundation of China, 111 Project (grant no. B07004), the Program for Changjiang Scholars, the Innovative Research Team in University (IRT1205) and the Central University Research Funds of China (buctrc201527).

Conflict of Interest

The authors declare no competing financial interests.

References

1. Liu J, Cao Z, Lu Y (2009) Functional Nucleic Acid Sensors. Chem Rev 109: 1948-1998.
2. Wu L,Qu X (2015) Cancer biomarker detection: recent achievements and challenges. Chem Soc Rev 44: 2963-2997.
3. Kimura M, Stone RC, Hunt SC (2010) Measurement of telomere length by the Southern blot analysis of terminal restriction fragment lengths. Nature Protocols 5: 1596-1607.
4. Mender I, Shay JW (2015) Telomere Restriction Fragment (TRF) Analysis. Bio-Protocol 5: e1658.
5. Cawthon RM (2002) Telomere measurement by quantitative PCR. Nucleic Acids Research 30: e47.
6. Cawthon RM (2009) Telomere length measurement by a novel monochrome multiplex quantitative PCR method. Nucleic Acids Research 37: e21.
7. Slijepcevic P (2001) Telomere length measurement by Q-FISH. Methods in Cell science an Official Journal of the Society forin Vitro Biology 23: 17-22.
8. Ferlicot S, Youssef N, Feneux D, Delhommeau F, ParadisV, et al. (2003) Measurement of telomere length on tissue sections using Quantitative Fluorescence *in Situ* Hybridization (Q-FISH). The Journal of Pathology 200: 661-666.
9. Brit-Compton B, Rowson J, Locke M, Mackenzie I, Kipling D, et al. (2006) Structural stability and chromosome-specific telomere length is governed by cis-acting determinants in humans. Human Molecular Genetics 15: 725-733.
10. Thompson DG, Enright A, Faulds K, Smith WE, Graham D (2008) Ultrasensitive DNA Detection Using Oligonucleotide-Silver Nanoparticle Conjugates. Anal Chem 80: 2805-2810.
11. Maxwell DJ, Taylor JR, Nie SJ (2002) Self-Assembled Nanoparticle Probes for Recognition and Detection of Biomolecules. J Am Chem Soc 124: 9606- 9607.
12. Lavis LD, Raines RT (2008) Bright Ideas for Chemical Biology. ACS Chem Biol 3: 142-155.
13. Rurack k (2001) Flipping the light switch 'on'--the design of sensor

molecules that show cation-induced fluorescence enhancement with heavy and transition metal ions. Spectrochim Acta Part A 57: 2161-2195.

14. Wilson WD, Tanious FA, Barton HJ, Strekowski L, Boykin DW (1989) Binding of 4',6-Diamidino-2-Phenylindole (DAPI) to GC and mixed sequences in DNA: intercalation of a classical groove-binding molecule. J Am Chem Soc 111: 5008-5010.

15. Holmlin RE, Barton JK (1995) Os(phen)2(dppz)2+: A Red-Emitting DNA Probe. Inorg Chem 34: 7-8.

16. Russell WC, Newman C, Williamson DH (1975) A simple cyto chemical technique for demonstration of DNA in cells infected with mycoplasmas and viruses. Nature 253: 461-462.

17. Pal N, Verma SD, Sen S (2010) Probe Position Dependence of DNA Dynamics: Comparison of the Time-Resolved Stokes Shift of Groove-Bound to Base-Stacked Probes. J Am Chem Soc 132: 9277-9279.

18. Vlieghe D, Sponer J, Van Meervelt L (1999) Crystal Structure of d(GGCCAATTGG) Complexed with DAPI Reveals Novel Binding Mode. Biochemistry 38: 16443-16451.

19. Kim SK, Eriksson S, Kubista M, Norden B (1995) Interaction of 4',6-diamidino-2-phenylindole (DAPI) with poly[d(G-C)2] and poly[d(G-m5C)2]: evidence for major groove binding of a DNA probe. J Am Chem Soc 115: 3441-3447.

20. Trotta E, Paci M (1998) Solution structure of DAPI selectively bound in the minor groove of a DNA T·T mismatch-containing site: NMR and molecular dynamics studies. Nucleic Acids Research 26: 4706-4713.

21. Tanious FA, Veal JM, Buczak H, Ratmeyer LS, Wilson WD (1992) DAPI (4',6-diamidino-2-phenylindole) binds differently to DNA and RNA: minor-groove binding at AT sites and intercalation at AU sites. Biochemistry 31: 3103-3112.

22. Williams GR, O'Hare D (2006) Towards understanding, control and application of layered double hydroxide chemistry. J Mater Chem 16: 3065-3074.

23. Fogg AM, Freij AJ, Parkinson GM (2002) Synthesis and Anion Exchange Chemistry of Rhombohedral Li/Al Layered Double Hydroxides. Chem. Mater 14: 232-234.

24. Wang Q, O'Hare D (2012) Recent Advances in the Synthesis and Application of Layered Double Hydroxide (LDH) Nanosheets. Chemical Reviews 12: 4124-4155.

25. Adachi-Pagano M, Forano C, Besse JP (2000) Delamination of layered double hydroxides by use of surfactants. Chem. Commun 1: 91-92.

26. Ma RZ, Sasaki T (2012) Synthesis of LDH Nanosheets and their Layer-by-Layer Assembly. Recent Patents on Nanotechnology 6: 159-168.

27. Li L, Ma RZ, Ebina Y, Iyi N, Sasaki T (2005) Positively Charged Nanosheets Derived via Total Delamination of Layered Double Hydroxides. Chem Mater 17: 4386-4391.

28. Gardner E, Huntoon KM, Pinnavaia TJ (2001) Direct Synthesis of Alkoxide-Intercalated Derivatives of Hydrocalcite-like Layered Double Hydroxides: Precursors for the Formation of Colloidal Layered Double Hydroxide Suspensions and Transparent Thin Films. Adv Mater 13: 1263-1266.

29. Li S, Li J, Wang CJ, Wang Q, Cader MZ, et al. (2013) Cellular uptake and gene delivery using layered double hydroxide nanoparticles. J Mater Chem B 1: 61-68.

30. Shi WY, Jia YK, Xu SM, Li ZX, Fu Y, et al. (2014) A Chiroptical Switch Based on DNA/Layered Double Hydroxide Ultrathin Films. Langmuir 30: 12916-12922.

31. Desigaux L, Belkacem MB, Richard P, Cellier J, Léone P, et al. (2006) Self-assembly and characterization of layered double hydroxide/DNA hybrids. Nano. Letters 6: 199-204.

32. Chen L, Sun K, Li P, Fan X, Sun J, et al. (2013) DNA-enhanced peroxidase-like activity of layered double hydroxide Nano sheets and applications in H_2O_2 and glucose sensing. Nanoscale 5: 10982-10988.

33. Baccar ZM, Caballero D, Eritja R, Errachid A (2012) Development of an impedimetric DNA-biosensor based on layered double hydroxide for the detection of long ssDNA sequences. Electrochimica Acta 74: 123-129.

34. Li SD, Lu J, Ma HK, Xu J, Yan DP, et al. (2011) Ordered Blue Luminescent Ultrathin Films by the Effective Coassembly of Tris(8-hydroxyquinolate-5-sulfonate) aluminum and Polyanions with Layered Double Hydroxides. Langmuir 27: 11501-11507.

35. Yan DP, Lu J, Chen L, Qin SH, Ma J, et al. (2010) A strategy to the ordered assembly of functional small cations with layered double hydroxides for luminescent ultra-thin films. Chem Commun 46: 5912-5914.

36. Qin Y, Shi J, Gong X, Tian Z, Zhang P, Lu J (2016) A Luminescent Inorganic/Organic Composite Ultrathin Film Based on a 2D Cascade FRET Process and Its Potential VOC Selective Sensing Properties. Adv Funct Mater 26: 6752-6759.

37. Zhao Y, Li F, Zhang R, Evans DG, Duan X (2002) Preparation of Layered Double-Hydroxide Nanomaterials with a Uniform Crystallite Size Using a New Method Involving Separate Nucleation and Aging Steps. Chem Mater 14: 4286- 4291.

38. Zhang P, Hu Y, Ma R, Li L, Lu J (2017) Enhanced green fluorescence protein/layered double hydroxide composite ultrathin films: bio-hybrid assembly and potential application as a fluorescent biosensor. J Mater Chem B 5: 160-166.

39. Biancardi A, Biver T, Secco F, Mennucci B (2013) An investigation of the photophysical properties of minor groove bound and intercalated DAPI through quantum-mechanical and spectroscopic tools. Phys Chem Chem Phys 15: 4596-4603.

40. Baraldi PG. Bovero A, Fruttarolo F, Preti D, Tabrizi MA, et al. (2004) DNA minor groove binders as potential antitumor and antimicrobial agents. Med Res Rev 24: 475-528.

41. Cosa G, Focsaneanu KS, McLean JRN, McNamee JP, Scaiano JC (2001) Photophysical Properties of Fluorescent DNA-dyes Bound to Single- and Double-stranded DNA in Aqueous Buffered Solution. Photochem Photobiol 73: 58-599.